

Inverse Chameleon Mechanism and Mass Limits for Compact Stars

Hao Wei* and Zhong-Xi Yu†

School of Physics, Beijing Institute of Technology, Beijing 100081, China

ABSTRACT

As is well known, there are various mass limits for compact stars. For example, the maximum mass for non-rotating white dwarfs is given by the famous Chandrasekhar limit about $1.4M_{\odot}$ (solar masses). Although the mass limit for neutron stars is not so clear to date, one of the widely accepted values is about $2.1M_{\odot}$. Recently, challenges to these mass limits appeared. Motivated by the super-Chandrasekhar mass white dwarfs with masses up to $2.4 \sim 2.8M_{\odot}$, and compact objects (probably neutron stars) in the mass gap (from $2.5M_{\odot}$ or $3M_{\odot}$ to $5M_{\odot}$) inferred from gravitational waves detected by LIGO/Virgo in the third observing run (O3), we reconsider the mass limits for compact stars in the present work. Without invoking strong magnetic field and/or exotic equation of state (EOS), we try to increase the mass limits for compact stars in modified gravity theory. In this work, we propose an inverse chameleon mechanism, and show that the fifth-force mediated by the scalar field can evade the severe tests on earth, in solar system and universe, but manifest itself in compact stars such as white dwarfs and neutron stars. The mass limits for compact stars in the inverse chameleon mechanism can be easily increased to $3M_{\odot}$, $5M_{\odot}$ or even larger. We argue that the inverse chameleon mechanism might be constrained by the observations of exoplanets orbiting compact stars (such as white dwarfs and neutron stars), and gravitational waves from the last stage of binary compact star coalescence.

PACS numbers: 04.50.Kd, 97.20.Rp, 95.36.+x, 97.60.Jd, 04.40.Dg

* Corresponding author; email address: haowei@bit.edu.cn

† email address: 547410406@qq.com

I. INTRODUCTION

As is well known, when a massive star ends, the stellar core remnant might form a compact object such as white dwarf, neutron star, and black hole [1–3]. At this stage, fusion reactions in the star stopped, and hence gravitational collapse must take place. If the mass of star is less than about $10M_{\odot}$ (solar masses), a white dwarf will be formed when gravitational collapse is eventually balanced by electron degeneracy pressure. As is well known, there is a maximum mass for non-rotating white dwarfs, namely the Chandrasekhar limit [4–7], whose currently accepted value is about $1.4M_{\odot}$. A white dwarf with a mass larger than the Chandrasekhar limit is subject to further gravitational collapse, and hence evolves into a neutron star. Neutron stars are supported against further collapse by neutron degeneracy pressure and repulsive nuclear forces. There is also a maximum mass for non-rotating neutron stars [1–3], namely the Tolman-Oppenheimer-Volkoff (TOV) limit. However, this mass limit is not so clear to date [8–10]. One of the widely accepted values is about $2.1M_{\odot}$ [8–10]. A recent estimate puts the upper limit at $2.16M_{\odot}$ [11]. To date, the maximum observed mass of neutron star is about $2.14M_{\odot}$ for PSR J0740+6620 discovered in September 2019 [12]. If exotic equation of state (EOS) is allowed, this mass limit might be $2.2M_{\odot}$, $2.5M_{\odot}$ or even higher (see e.g. [13, 14]). A neutron star with a mass larger than the TOV limit is subject to further gravitational collapse, and then forms a black hole. However, hypothetical intermediate-mass stars such as quark star, boson star, electroweak star and gravastar might exist between neutron star and black hole, although none of them has been discovered to date. Of course, there must also be mass limits for these hypothetical compact stars, beyond which they collapse into a black hole.

Recently, challenges to these mass limits appeared. It is widely accepted that type Ia supernovae (SNIa) are explosions of carbon-oxygen white dwarfs. For the first time, the progenitor of a very bright SNIa, namely SNLS-03D3bb (SN 2003fg), was found to be a super-Chandrasekhar mass white dwarf in 2006 [15]. In fact, the mass of this white dwarf is about $2.1M_{\odot}$, highly exceeding the Chandrasekhar mass limit (about $1.4M_{\odot}$). Later, more super-Chandrasekhar mass white dwarfs were found to be the progenitors of very bright SNIa, for example, SN 2006gz, SN 2007if, and SN 2009dc, as summarized in e.g. [16, 17]. These super-Chandrasekhar mass white dwarfs have masses up to $2.4 \sim 2.8M_{\odot}$. In addition, a super-Chandrasekhar nucleus of the planetary nebula Henize 2-428 with a combined mass of $1.76M_{\odot}$ was found [18]. To date, fewer than ten candidates of super-Chandrasekhar mass white dwarfs are under consideration, for example, the progenitors of SN 2012dn, SN 2011aa, SN 2011hr, SN 2004gu, LSQ12gdj, and iPTF13asv, as summarized in e.g. [19, 20]. These super-Chandrasekhar mass white dwarfs clearly require a new theoretical mass limit for white dwarfs.

On the other hand, direct detections of gravitational waves (GWs) become available since September 2015 [21, 22]. In the LIGO/Virgo classification, a “MassGap” system refers to a binary system with at least one compact object whose mass is in the range of $3 \sim 5M_{\odot}$ [23]. A natural question is that if a MassGap GW event has been detected, what is the compact object with a mass between $3M_{\odot}$ and $5M_{\odot}$? It might be a large mass neutron star, or a small mass black hole. The difference is whether there is electromagnetic counterpart or not. On 16 December 2019, LIGO/Virgo detected a GW event S191216ap, and initially classified it as MassGap with a $> 99\%$ probability (GCN circular 26454) [24, 25]. Soon, the IceCube Collaboration claimed that a neutrino counterpart associated with S191216ap was found (GCN circular 26460) [24]. Then, the HAWC Collaboration claimed that a gamma-ray counterpart associated with S191216ap was also found (GCN circular 26472) [24]. Since two electromagnetic counterparts were claimed, the compact object in MassGap cannot be a black hole, and it is probably a neutron star with a mass larger than $3M_{\odot}$, exceeding the theoretical mass limits for neutron stars mentioned above. Unfortunately, LIGO/Virgo changed the classification of S191216ap to BBH ($> 99\%$) on 19 December 2019 (GCN circular 26570) [24, 25], and then the story ended. Anyway, this motivates us to reconsider the theoretical mass limit for neutron stars. We should be ready in advance for a MassGap neutron star ($M > 3M_{\odot}$) associated with electromagnetic counterparts in the future.

Another very important GW event is GW190814 [26–28]. LIGO/Virgo initially classified this event as MassGap ($> 99\%$) on 14 August 2019 (GCN circular 25324) [26, 27], and then changed it to NSBH ($> 99\%$) on the next day (GCN circular 25333) [26, 27]. After detailed analyses, LIGO/Virgo found in [28] that it came from the coalescence of a $23M_{\odot}$ black hole with a $2.6M_{\odot}$ compact object (note that in the press release [29], LIGO/Virgo still classified the $2.6M_{\odot}$ compact object in the mass gap). Because no black hole with a mass less than $5M_{\odot}$ was observed before, if the $2.6M_{\odot}$ compact object is a black hole, could it be a primordial black hole? As mentioned above, the maximum observed mass of

neutron star is about $2.14M_{\odot}$ to date [12]. The mass of this compact object ($2.6M_{\odot}$) also well exceeds the widely accepted mass limit for neutron stars mentioned above (about $2.16M_{\odot}$). Unfortunately, no electromagnetic counterpart associated with GW190814 was claimed [26] (but see also e.g. [30]). So, none can tell whether this $2.6M_{\odot}$ compact object is a neutron star or not. Anyway, this motivates us again to reconsider the theoretical mass limit for neutron stars.

In the literature, there are various scenarios to increase the mass limits for compact stars such as white dwarfs and neutron stars. Strong magnetic field and/or exotic EOS are frequently invoked in many scenarios (see e.g. [31–35] and [14, 36–40]). Another type of scenarios is to consider compact stars in modified gravity theories. If gravitational force is weakened (with respect to general relativity), the mass limits for compact stars can accordingly increase, as expected. We refer to e.g. [41] for a comprehensive review. However, it is worth noting that in modified gravity theories, gravitational force is modified on all scales, not only in compact stars but also in solar system and universe. In fact, many modified gravity theories, in which the mass limits for compact stars could be considerably increased, will significantly deviate from general relativity (GR), and hence they are difficult to simultaneously evade the severe tests on earth and in solar system (as well as the cosmological tests).

The key is to make gravity environment-dependent. One of this kind of modified gravity theories is the well-known chameleon mechanism [42–47], which was proposed mainly for cosmology. This mechanism can hide dark energy (played by a scalar field coupling to matter, namely the so-called chameleon field) on earth and in solar system, but show it on cosmological and galactic scales. The mass of scalar field depends on the ambient matter density. On earth and in solar system, where the matter density is high, the scalar field is massive, and hence the fifth-force range is short enough to evade the severe tests on earth and in solar system. On cosmological and galactic scales, where the matter density is low, the mass of scalar field is light, and hence the fifth-force range is long enough to drive the cosmic acceleration or the evolution of the fine-structure “constant”. Unfortunately, this chameleon mechanism cannot be used to increase the mass limits for compact stars. The matter density is very high in compact stars, and hence the range of fifth-force mediated by the scalar field is too short to manifest itself.

In the present work, we try to invert the chameleon mechanism. In our inverse chameleon mechanism, we will show the fifth-force mediated by the scalar field in compact stars, and hide it on earth, in solar system and universe. So, the mass limits for compact stars can be significantly increased in the inverse chameleon mechanism, and simultaneously evade the severe tests on earth and in solar system (as well as the cosmological tests).

The rest of this paper is organized as follows. In Sec. II, we briefly review the key points of chameleon mechanism. In Secs. III and IV, we propose our inverse chameleon mechanism. We present the solutions for a compact object, and show that the fifth-force mediated by the scalar field can evade the severe tests on earth, in solar system and universe, but manifest itself in compact stars such as white dwarfs and neutron stars. In Sec. V, we derive the new mass limits for white dwarfs and other compact stars in the inverse chameleon mechanism. In fact, they can be easily increased, exceeding the mass gap, namely $M > 3M_{\odot}$ or even larger. In Sec. VI, some brief concluding remarks are given.

II. THE KEY POINTS OF CHAMELEON MECHANISM

At first, we briefly review the key points of chameleon mechanism, following e.g. [42–47]. In the Einstein frame, the canonical scalar field ϕ (namely the chameleon field) is governed by the action

$$S = \int d^4x \sqrt{-g} \left[\frac{M_{pl}^2}{2} R - \frac{1}{2} (\partial\phi)^2 - V(\phi) \right] + S_m(g^J), \quad (1)$$

in which matter fields described by S_m couple to ϕ through the conformal factor $A(\phi)$ implicit in the Jordan-frame metric [46]

$$g_{\mu\nu}^J = A^2(\phi) g_{\mu\nu}, \quad (2)$$

and $M_{pl} \equiv (8\pi G)^{-1/2}$ is the reduced Planck mass, g is the determinant of the metric $g_{\mu\nu}$, R is the Ricci scalar. We use the units $\hbar = c = 1$, and the metric convention $(-, +, +, +)$. In principle, one

can allow different couplings to the various matter fields through $g_{\mu\nu}^{J(i)} = A_i^2(\phi) g_{\mu\nu}$, explicitly violating the equivalence principle, as in e.g. [42–44, 47]. For simplicity, following e.g. [46], we only consider the simplest case of a universal coupling in this work, without violating the equivalence principle. From the action (1), the equation of motion for ϕ is given by [46, 48]

$$\square\phi = V_{,\phi} + A_{,\phi}\rho = V_{\text{eff},\phi}, \quad (3)$$

where \square is the d'Alembertian, $f_{,\phi}$ denotes the derivative of any function f with respect to ϕ , and the effective potential is defined by

$$V_{\text{eff}}(\phi) = V(\phi) + A(\phi)\rho. \quad (4)$$

The matter density ρ is related to the Einstein-frame matter density ρ_E and the Jordan-frame matter density ρ_J by $\rho = \rho_E/A = A^3\rho_J$ [46], so that ρ is conserved in the Einstein frame [42–47]. On the other hand, the acceleration of a test particle is influenced by the scalar field according to [46, 48]

$$\mathbf{a} = -\nabla\Phi_N - \frac{d\ln A(\phi)}{d\phi}\nabla\phi = -\nabla(\Phi_N + \ln A(\phi)), \quad (5)$$

where Φ_N is the (Einstein-frame) Newtonian potential, which satisfies [46, 48]

$$\nabla^2\Phi_N = 4\pi G\rho_E = 4\pi GA\rho. \quad (6)$$

In the chameleon mechanism, an exponential coupling is usually considered, i.e. [42–47]

$$A(\phi) = \exp(\beta\phi/M_{pl}), \quad (7)$$

where $\beta \sim \mathcal{O}(1)$ is a dimensionless constant. Clearly, $A(\phi)$ is monotonically increasing. The potential $V(\phi)$ is assumed to be of the runaway form, so that it is monotonically decreasing. The fiducial example is an inverse power-law potential [42, 43, 46]

$$V(\phi) = \mathcal{M}^4 (\mathcal{M}/\phi)^n, \quad (8)$$

where \mathcal{M} has units of mass, and n is a positive constant. So, the effective potential V_{eff} can develop a minimum at some finite field values ϕ_{min} in the presence of background matter density. It is easy to find $\phi_{\text{min}} \propto \rho^{-1/(n+1)}$ [46] by requiring $V_{\text{eff},\phi}(\phi_{\text{min}}) = 0$. Note that we only consider the case of $\phi \ll M_{pl}$ throughout this work, following e.g. [42–47]. The mass of small fluctuations about the minimum at ϕ_{min} for the canonical scalar field ϕ is defined as usual [42–47]

$$m_\phi^2 \equiv V_{\text{eff},\phi\phi}(\phi_{\text{min}}) \geq 0. \quad (9)$$

Noting ρ in the effective potential given by Eq. (4), the originally massless scalar field ϕ acquires a mass depending on the local matter density. Substituting ϕ_{min} into Eq. (9), and noting $\phi \ll M_{pl}$, we find that $m_\phi^2 \propto \rho^{(n+2)/(n+1)}$ [46] is an increasing function of the background density. So, on earth and in solar system, where the matter density is high, the scalar field is massive, and hence the fifth-force range is short enough to evade the severe tests on earth and in solar system. On cosmological and galactic scales, where the matter density is low, the mass of scalar field is light, and hence the fifth-force range is long enough to drive the cosmic acceleration or the evolution of the fine-structure “constant”. We refer to e.g. [42, 43, 45] for the detailed magnitude analyses to evade the tests on earth and in solar system. The key point is to require the range of fifth-force mediated by the scalar field ϕ in the atmosphere $m_{\text{atm}}^{-1} \lesssim \mathcal{O}(1 \text{ mm})$ [42, 43, 45]. For n and β of order unity, it can be translated into a constraint on the scale \mathcal{M} , namely $\mathcal{M} \lesssim 10^{-3} \text{ eV} \sim (1 \text{ mm})^{-1}$ [42, 43].

The screening of fifth-force mediated by the scalar field ϕ can also be seen from the solutions for a compact object [42, 43]. The key is the so-called “thin-shell” effect. We refer to [42, 43] for the explicit solutions. The exterior solution for a compact object having the thin-shell effect is suppressed by a factor $3\Delta R_c/R_c \ll 1$ with respect to the exterior solution for a compact object without the thin-shell effect. This effect can be understood from the physical picture following e.g. [43, 46]. If the object is sufficiently massive such that deep inside the object the scalar field minimizes the effective potential for the interior

density, the mass of scalar field is relatively large inside the object, and hence the fifth-force range is relatively short. Thus, the contribution from the core to the exterior profile is significantly suppressed. Only the contribution from a thin shell beneath the surface contributes considerably to the exterior profile [46]. This is the physical reason of the thin shell effect.

In the literature, there are many interesting works used the chameleon mechanism. Of course, most of them concern cosmology. Unfortunately, the chameleon mechanism cannot be used to increase the mass limits for compact stars, as mentioned in Sec. I. The matter density is very high in compact stars, and hence the range of fifth-force mediated by the scalar field is too short to manifest itself. Therefore, we should find a way out.

III. INVERSE CHAMELEON MECHANISM

A. The ingredients of inverse chameleon mechanism

We try to invert the chameleon mechanism. Since a canonical scalar field (akin to quintessence) is used in the chameleon mechanism, we instead consider a non-canonical scalar field (akin to phantom) [49] in our inverse chameleon mechanism. As is well known, in cosmology, phantom is almost the inverse of quintessence. While the kinetic energy term of quintessence is positive, it is negative instead in the case of phantom. So, the behaviors of phantom and quintessence are almost inverse. For example, in cosmology where ϕ depends only on the time t , phantom rests at the maximum of its potential, while quintessence rests at the minimum. Naively, let us begin our inverse chameleon mechanism with the action

$$S = \int d^4x \sqrt{-g} \left[\frac{M_{pl}^2}{2} R + \frac{1}{2} (\partial\phi)^2 - V(\phi) \right] + S_m(g^J), \quad (10)$$

where ϕ is a non-canonical scalar field (akin to phantom) instead, and $g_{\mu\nu}^J$ takes the same form of Eq. (2). The sign of $(\partial\phi)^2$ term is opposite to the one in Eq. (1). So, the equation of motion for ϕ is given by

$$-\square\phi = V_{,\phi} + A_{,\phi}\rho = V_{\text{eff},\phi}, \quad (11)$$

which is also opposite to Eq. (3), while V_{eff} takes the same form of Eq. (4). Of course, the acceleration of a test particle influenced by the scalar field also takes the same form of Eq. (5), while Eq. (6) still holds for the (Einstein-frame) Newtonian potential Φ_N .

Our goal is to make the mass of the scalar field small (large) when the ambient matter density ρ is large (small), in opposite to the chameleon mechanism. Unlike a canonical scalar field (akin to quintessence), the mass of a non-canonical scalar field (akin to phantom) is defined about the maximum at ϕ_{max} , i.e.

$$m_\phi^2 \equiv -V_{\text{eff},\phi\phi}(\phi_{\text{max}}) \geq 0, \quad (12)$$

since $V_{\text{eff},\phi\phi}$ is negative at the maximum of the effective potential. Naively, we consider

$$V(\phi) = V_0 \phi^s, \quad A(\phi) = \exp(\beta\phi/M_{pl}), \quad (13)$$

where V_0 has units of $[\text{mass}]^{4-s}$, and $\beta \sim \mathcal{O}(1)$ is a dimensionless constant. Note that we only consider the case of $\phi \ll M_{pl}$ throughout this work, following e.g. [42–47]. Requiring $V_{\text{eff},\phi}(\phi_{\text{max}}) = 0$, we find

$$\phi_{\text{max}} = \left(-\frac{\beta\rho}{sV_0M_{pl}} \right)^{1/(s-1)}. \quad (14)$$

To be a maximum, it is required that

$$V_{\text{eff},\phi\phi}(\phi_{\text{max}}) = V_0 s(s-1) \left(-\frac{\beta\rho}{sV_0M_{pl}} \right)^{(s-2)/(s-1)} \leq 0. \quad (15)$$

To avoid complex number, $-\beta\rho/(sV_0M_{pl}) > 0$ is required. So, we have $V_0 s(s-1) \leq 0$. Noting that

$$m_\phi^2 = -V_{\text{eff},\phi\phi}(\phi_{\text{max}}) \propto \rho^{(s-2)/(s-1)}, \quad (16)$$

$(s-2)/(s-1) < 0$ is required to make m_ϕ being a decreasing function of ρ . So, we should set

$$1 < s < 2, \quad V_0 \leq 0, \quad \beta > 0, \quad (17)$$

in the inverse chameleon mechanism. One might worry about the potential $V(\phi) = V_0 \phi^s$ in Eq. (13), since it might become complex number for $\phi < 0$. To extend the relevant range of ϕ to the negative region, we can instead use $V(\phi) = V_0 |\phi|^s$, which is still the same $V(\phi) = V_0 \phi^s$ for $\phi \geq 0$. But for $\phi < 0$, noting that $V_0 \leq 0$, $V(\phi) = V_0 (-\phi)^s$ is monotonically decreasing as $\phi \rightarrow -\infty$. Because $A(\phi)$ is also monotonically decreasing as $\phi \rightarrow -\infty$, the maximum of V_{eff} certainly does not appear in the region of $\phi < 0$. In fact, noting Eqs. (17) and (14), $\phi_{\text{max}} > 0$ always. So, it is safe to use $V(\phi) = V_0 \phi^s$ in the range of $0 \leq \phi \ll M_{pl}$ (note that a minimum will develop for $\phi \gtrsim M_{pl}$ beyond our scope $\phi \ll M_{pl}$).

B. Constraints on model parameters

In the inverse chameleon mechanism, the mass of the scalar field m_ϕ is a decreasing function of the local matter density ρ , as shown in Eq. (16) with $1 < s < 2$. So, m_ϕ can be very small in compact stars such as white dwarfs and neutron stars where the matter density is very high, and hence the fifth-force range is long enough (even far beyond the radius of compact star) to manifest itself. On the contrary, m_ϕ can be large on earth, in solar system and universe where the matter density is relatively low, so that the fifth-force range is short enough to evade the severe tests.

Noting $V_0 \leq 0$, we recast the potential $V(\phi)$ as

$$V(\phi) = V_0 \phi^s = -\mathcal{M}^4 (\phi/\mathcal{M})^s, \quad (18)$$

where \mathcal{M} has units of mass. In this case, we have

$$m_\phi^{-1} = (s(s-1))^{-1/2} \mathcal{M}^{(s-4)/(2(s-1))} \left(\frac{\beta\rho}{sM_{pl}} \right)^{(2-s)/(2(s-1))}, \quad (19)$$

which characterizes the fifth-force range. Note that the mean densities of atmosphere, earth and sun are $\rho_{\text{atm}} \simeq 1.2 \times 10^{-3} \text{ g/cm}^3$, $\rho_\oplus \simeq 5.514 \text{ g/cm}^3$ and $\rho_\odot \simeq 1.408 \text{ g/cm}^3$, respectively. The densest object on earth is the metal Osmium (Os) with $\rho_{\text{Os}} = 22.59 \text{ g/cm}^3$. For magnitude estimate, it is convenient to simply use $\rho_{\text{metal}} \sim \mathcal{O}(10 \text{ g/cm}^3)$. Noting Eq. (19) with $1 < s < 2$, m_ϕ^{-1} is a increasing function of ρ . If the fifth-force range is short enough to evade the severe tests for metal, it holds on earth, in solar system and universe where $\rho < \rho_{\text{metal}}$. Similarly, if the fifth-force range is long enough to manifest itself for white dwarfs ($\rho_{\text{WD}} \sim 10^6 \text{ g/cm}^3$), it holds for all compact stars with much higher densities.

Let us find the constraints on model parameters. It is worth noting that

$$m_{\text{WD}}^{-1} \sim m_{\text{metal}}^{-1} (\rho_{\text{WD}}/\rho_{\text{metal}})^{(2-s)/(2(s-1))} \sim m_{\text{metal}}^{-1} \cdot 10^{5(2-s)/(2(s-1))}, \quad (20)$$

which increases as $s \rightarrow 1$. According to e.g. [42–47], $m_\phi^{-1} \lesssim \mathcal{O}(1 \text{ mm})$ is enough to evade the fifth-force tests on earth and in solar system. So, we consider $m_{\text{metal}}^{-1} \sim 1 \text{ mm}$ for magnitude estimate. In this case, $m_{\text{WD}}^{-1} \sim 10^{33/2} \text{ km}$, 10^4 km , $10^{-1/6} \text{ km}$, $10^{-9/4} \text{ km}$, $10^{-7/2} \text{ km}$ for $s = 1.1, 1.2, 1.3, 1.4, 1.5$, respectively. Noting that the typical radius of white dwarfs $\sim \mathcal{O}(10^3 \text{ km})$, it is suitable to use $1 < s \lesssim 1.2$ to manifest the fifth-force in white dwarfs. On the other hand, for earth, sun, diamond, ceramics, silicon, and metals of $\rho \sim \mathcal{O}(1 \text{ g/cm}^3)$, we have $m_\oplus^{-1} \sim m_\odot^{-1} \sim m_{\text{light metal}}^{-1} \sim m_{\text{metal}}^{-1} \cdot 10^{(s-2)/(2(s-1))} \lesssim 10^{-2} m_{\text{metal}}^{-1} \sim 10^{-2} \text{ mm}$ for $1 < s \lesssim 1.2$. Similarly, $m_{\text{atm}}^{-1} \sim m_{\text{metal}}^{-1} \cdot 10^{2(s-2)/(s-1)} \lesssim 10^{-8} m_{\text{metal}}^{-1} \sim 10^{-8} \text{ mm}$ for $1 < s \lesssim 1.2$. Let us turn to the scale \mathcal{M} . Noting Eq. (19), $m_\phi^{-1} \lesssim \mathcal{O}(1 \text{ mm})$ to evade the fifth-force tests on earth and in solar system can be translated to $\mathcal{M} \gtrsim 10 \text{ mm}^{-1} \sim 2 \times 10^{-3} \text{ eV}$ for $s = 1.2$, $\beta = 1/2$, and $\rho \sim 20 \text{ g/cm}^3$. Of course, one can instead take a much conservative value, e.g. $m_\phi^{-1} \lesssim \mathcal{O}(1 \mu\text{m})$, to evade the fifth-force tests on earth and in solar system. We consider $m_{\text{metal}}^{-1} \sim 1 \mu\text{m}$ for magnitude estimate. In this case, $s = 1.2$ is not enough to make m_{WD}^{-1} larger than the typical radius of white dwarfs. But $s = 1.1$ is certainly enough, since the corresponding $m_{\text{WD}}^{-1} \sim 10^{27/2} \text{ km}$. On the other hand, we find that $\mathcal{M} \gtrsim 15 \text{ mm}^{-1} \sim 3 \times 10^{-3} \text{ eV}$ for $s = 1.1$, $\beta = 1/2$, and $\rho \sim 10 \text{ g/cm}^3$. In summary, we can always use a s close to 1 and a higher $\mathcal{M} \gtrsim \mathcal{O}(10 \text{ mm}^{-1}) \sim \mathcal{O}(10^{-3} \text{ eV})$ to evade the tests on earth, in solar system and universe, but manifest the fifth-force in compact stars such as white dwarfs and neutron stars.

IV. THE SOLUTIONS FOR A COMPACT OBJECT

A. The qualitative description

Here, we derive the approximate solutions of the scalar field ϕ in the inverse chameleon mechanism for a spherical homogeneous isolated compact object, similar to the case of chameleon mechanism [42, 43]. Let the radius, density and total mass of this object be R_c , ρ_c and $M_c = 4\pi\rho_c R_c^3/3$, respectively. We assume that it is immersed in a background of homogeneous density ρ_∞ (less than ρ_c usually), similar to objects in the atmosphere, earth in the solar plasma, sun and (compact) stars in the interstellar gas, galaxies in the intergalactic medium. So, the equation of motion in Eq. (11) for $\phi = \phi(r)$ becomes

$$\nabla^2\phi = \frac{d^2\phi}{dr^2} + \frac{2}{r}\frac{d\phi}{dr} = -V_{,\phi} - A_{,\phi}\rho = -V_{\text{eff},\phi}, \quad (21)$$

where $\rho(r) = \rho_c$ for $r < R_c$ and $\rho(r) = \rho_\infty$ for $r > R_c$. It is worth noting that at $r = R_c$, the matter density ρ jumps from ρ_c to ρ_∞ . Accordingly, the effective potential V_{eff} also undergoes a jump, while its shape changes. Noting $\phi_{\text{max}} \propto \rho^{1/(s-1)}$ from Eq. (14) and $1 < s < 2$, ϕ_{max} decreases when the matter density ρ jumps from ρ_c to ρ_∞ . This means that V_{eff} jumps to the left side, in contrast to the case of chameleon mechanism [42, 43]. We present the demonstrational plots of V_{eff} in Fig. 1 (not to scale). We denote the field values minimizing V_{eff} as ϕ_c and ϕ_∞ for $r < R_c$ and $r > R_c$, respectively. Eq. (21) is a second order differential equation, and hence two boundary conditions are needed. Following [42, 43], we require that the solution should be non-singular at the origin,

$$d\phi/dr = 0 \quad \text{at} \quad r = 0, \quad (22)$$

and the fifth-force tends to zero ($d\phi/dr \rightarrow 0$, n.b. Eq. (5) still holds in the inverse chameleon mechanism) as $r \rightarrow \infty$. The latter is actually equivalent to

$$\phi \rightarrow \phi_\infty \quad \text{as} \quad r \rightarrow \infty, \quad (23)$$

which is natural since $\rho = \rho_\infty$ at infinity.

Following e.g. [42, 43], to get an intuition, it is useful to think of r as a “time” coordinate and ϕ as the “position” of a “particle”, treating Eq. (21) as a dynamical problem in classical mechanics. In this language, $d^2\phi/dr^2$ and $d\phi/dr$ are the “acceleration” and the “speed”, respectively, while $-V_{\text{eff},\phi}$ is a “time-dependent force” and $(2/r)d\phi/dr$ is a “speed-dependent damping term” (or “friction”). At the initial “time” $r = 0$, the “particle” is at rest (see Eq. (22)), and begins from the initial value $\phi_i \equiv \phi(r = 0)$. For small r , the “damping term” ($\propto 1/r$) is large, and hence the “particle” is frozen at $\phi = \phi_i$ for a long “time” ($0 < r < R_{\text{roll}}$). The frozen “time” (i.e. the value of R_{roll}) depends on the slope of the potential, namely the “driving term” $-V_{\text{eff},\phi}$. Note that $V_{\text{eff},\phi} \simeq 0$ for a ϕ_i close to ϕ_c , but it is large enough for a ϕ_i sufficiently displaced from ϕ_c . In fact, they correspond to the cases of “thin shell” and “thick shell”, respectively. As r increases, the “damping term” decreases. Finally, at $r \simeq R_{\text{roll}}$, the “damping term” becomes smaller than the “driving term” $-V_{\text{eff},\phi}$, and then the “particle” begins to roll down the effective potential V_{eff} , as shown in the right panel of Fig. 1. Later, it arrives at $r = R_c$, where V_{eff} suddenly changes as ρ jumps from ρ_c to ρ_∞ . But ϕ and $d\phi/dr$ are continuous at $r = R_c$.

Outside the compact object, the “particle” changes to climb up the new V_{eff} as shown in the left panel of Fig. 1. At this stage, the “force” $-V_{\text{eff},\phi}$ changes its sign, and help the “friction” to pull back the “particle”. But the “speed” of the “particle” is large enough compared to the new slope of the effective potential $V_{\text{eff},\phi}$, and hence it keeps moving leftwards by inertia. At the first stage outside the compact object ($R_c < r < R_t$), because the “friction” $(2/r)d\phi/dr$ is much larger than $-V_{\text{eff},\phi}$ due to the relatively large “speed” $d\phi/dr$, the “force” $-V_{\text{eff},\phi}$ can be completely neglected (although $-V_{\text{eff},\phi} \not\approx 0$ if $\phi(r = R_c)$ is sufficiently far from ϕ_∞ , as shown in the left panel of Fig. 1). We call $R_c < r < R_t$ the transition region. As r increases, the “friction” $(2/r)d\phi/dr$ becomes small, because the “speed” $d\phi/dr$ is decelerated and $2/r$ decreases. Meanwhile, the slope of $V_{\text{eff},\phi}$ also tends to 0, as the “particle” climbs up V_{eff} outside the compact object, as shown in the left panel of Fig. 1. At the second stage ($r > R_t$), ϕ becomes fairly close to ϕ_∞ , while $-V_{\text{eff},\phi} \simeq 0$ indeed. In the end, it will reach ϕ_∞ as $r \rightarrow \infty$. At this stage, the “acceleration” $d^2\phi/dr^2$ and the “speed” $d\phi/dr$ tend to 0 (accordingly the “friction” $(2/r)d\phi/dr$ also

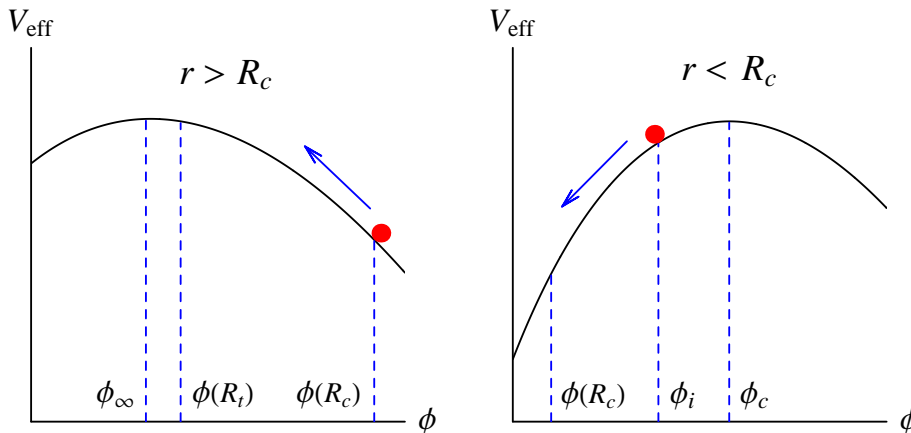


FIG. 1: The effective potential V_{eff} for a compact object of radius R_c is discontinuous at $r = R_c$, since the matter density $\rho = \rho_c$ for $r < R_c$ (right panel), and $\rho = \rho_\infty$ for $r > R_c$ (left panel). The scalar field $\phi(r)$ (red solid balls) rolls from ϕ_i to ϕ_∞ , as r runs from 0 to ∞ . Since $\phi_\infty < \phi_c$ for $\rho_\infty < \rho_c$ usually, it is more convenient to put the $r > R_c$ panel on the left side of the $r < R_c$ panel. The plots are not to scale. See Sec. IV for details.

tends to 0), so that the first order approximation of $-V_{\text{eff},\phi} \simeq 0$, namely $-V_{\text{eff},\phi\phi}(\phi - \phi_\infty) = m_\infty^2(\phi - \phi_\infty)$, makes sense. The width of transition region depends on the distance between $\phi(r = R_c)$ and ϕ_∞ . In the case of thin shell mentioned above, we will see that $|(\phi_c - \phi_\infty)/(6\beta M_{\text{pl}}\Phi_c)| \ll 1$ in the following (as in the case of chameleon mechanism [42, 43]). So, $\phi(r = R_c)$ between ϕ_c and ϕ_∞ is close enough to ϕ_∞ . Thus, the transition region can be ignored in the case of thin shell regime. On the contrary, there will be a considerable transition region in the case of thick shell regime.

B. The thin shell regime

As in the chameleon mechanism [42, 43], we consider the “thin shell” regime and the “thick shell” regime in our inverse chameleon mechanism, one by one. The thin shell regime is defined by $|\phi_i - \phi_c| \ll \phi_c$, namely ϕ_i is very close to ϕ_c . As mentioned above, due to the large “damping term” ($\propto 1/r$) and hence the “particle” is frozen at $\phi = \phi_i$ for a long “time”. So, in the frozen region we have

$$\phi(r) \simeq \phi_i \simeq \phi_c \quad \text{for } 0 < r < R_{\text{roll}}. \quad (24)$$

When $r \sim R_{\text{roll}}$, ϕ is still near ϕ_c but begins to roll, because the “damping term” $(2/r)d\phi/dr$ becomes relatively smaller and the “driving term” $-V_{\text{eff},\phi}$ makes sense, as mentioned above. In the rolling region $R_{\text{roll}} < r < R_c$, the slope of $V(\phi)$ is much smaller than the one of $A(\phi)\rho$ as soon as ϕ is displaced significantly from ϕ_c , similar to the case of chameleon mechanism [42, 43] (one can see this by simply plotting $A(\phi)\rho$ and $V(\phi)$ in the same plane versus ϕ). Thus, using $|V_{,\phi}| \ll A_{,\phi}\rho_c$, Eq. (21) can be approximated by

$$\nabla^2\phi = \frac{d^2\phi}{dr^2} + \frac{2}{r}\frac{d\phi}{dr} \simeq -A_{,\phi}\rho_c \simeq -\frac{\beta\rho_c}{M_{\text{pl}}}\left(1 + \frac{\beta\phi}{M_{\text{pl}}} + \dots\right), \quad (25)$$

where we have used $A(\phi)$ in Eq. (13), and considered its Taylor expansion up to the first order, noting $\beta\phi/M_{\text{pl}} \ll 1$, similar to e.g. [42, 43]. The approximate solution of Eq. (25) is given by

$$\phi(r) \simeq -\frac{\beta\rho_c}{3M_{\text{pl}}}\left(\frac{r^2}{2} + \frac{\hat{c}}{r}\right) + \bar{c} + \phi_c. \quad (26)$$

Note that ϕ and $d\phi/dr$ are continuous at $r = R_{\text{roll}}$. Requiring $d\phi/dr = 0$ and $\phi = \phi_c$ at $r = R_{\text{roll}}$, we find that $\hat{c} = R_{\text{roll}}^3$ and $\bar{c} = \beta\rho_c R_{\text{roll}}^2/(2M_{\text{pl}})$. So, in the rolling region we obtain

$$\phi(r) \simeq -\frac{\beta\rho_c}{3M_{\text{pl}}}\left(\frac{r^2}{2} + \frac{R_{\text{roll}}^3}{r}\right) + \frac{\beta\rho_c R_{\text{roll}}^2}{2M_{\text{pl}}} + \phi_c \quad \text{for } R_{\text{roll}} < r < R_c. \quad (27)$$

It is worth noting that the approximation of separating the solution for $0 < r < R_c$ into Eqs. (24) and (27) makes sense only if $R_c - R_{roll} \ll R_c$ (namely the shell is thin), for otherwise there is no clear separation between the two regions, and one needs a solution valid over the entire range $r < R_c$ [42, 43]. Then, the “particle” arrives at $r = R_c$, where the matter density ρ jumps from ρ_c to ρ_∞ , and ϕ changes to climb up the new V_{eff} with $\rho = \rho_\infty$, as shown in Fig. 1. As mentioned above, in the thin shell regime, the transition region can be ignored, because $\phi(r = R_c)$ is fairly close to ϕ_∞ . So, $-V_{\text{eff},\phi} \simeq 0$, and its first order approximation makes sense. Noting that ϕ is very close to ϕ_∞ , Eq. (21) becomes

$$\nabla^2 \phi = \frac{d^2 \phi}{dr^2} + \frac{2}{r} \frac{d\phi}{dr} = -V_{\text{eff},\phi} = -V_{\text{eff},\phi}(\phi_\infty) - V_{\text{eff},\phi\phi}(\phi_\infty)(\phi - \phi_\infty) + \dots \simeq m_\infty^2 (\phi - \phi_\infty), \quad (28)$$

where we have used Eq. (12). Its solution is given by

$$\phi(r) \simeq \frac{C_\infty e^{-m_\infty(r-R_c)}}{r} + \phi_\infty, \quad (29)$$

in which the divergent solution $\exp(m_\infty(r - R_c))/r$ has been excluded by the boundary condition in Eq. (23). The two unknowns C_∞ and R_{roll} can be determined by requiring $d\phi/dr$ and ϕ are continuous at $r = R_c$. Matching $d\phi/dr$ from Eqs. (27) and (29) at $r = R_c$ gives

$$\frac{\beta \rho_c}{3M_{pl}} \left(R_c - \frac{R_{roll}^3}{R_c^2} \right) = \frac{C_\infty}{R_c^2} (1 + m_\infty R_c). \quad (30)$$

In the case of chameleon mechanism [42, 43], $m_\infty R_c \ll 1$ because the mass of the scalar field is small when the local matter density ρ_∞ is low. However, in the inverse chameleon mechanism, $m_\infty R_c \gg 1$ because the mass of the scalar field is large when the local matter density ρ_∞ is low. This is a key difference between these two mechanisms. We can look at this point carefully. In the case of thin shell, the fifth-force range $m_c^{-1} \ll R_c$, while $m_\infty > m_c$ for $\rho_\infty < \rho_c$, since m_ϕ is a decreasing function of ρ in the inverse chameleon mechanism, as mentioned in Sec. III A. Thus, $m_\infty^{-1} < m_c^{-1} \ll R_c$ and hence $m_\infty R_c \gg 1$. So, in our case, from Eq. (30) we find that

$$C_\infty \simeq \frac{\beta \rho_c}{3M_{pl}} \frac{R_c^2}{m_\infty} \left(1 - \frac{R_{roll}^3}{R_c^3} \right) = \frac{\beta}{4\pi M_{pl}} \frac{M_c}{m_\infty R_c} \left(1 - \frac{R_{roll}^3}{R_c^3} \right) \simeq \frac{\beta}{4\pi M_{pl}} \frac{M_c}{m_\infty R_c} \left(\frac{3\Delta R_c}{R_c} \right), \quad (31)$$

where we have used

$$\frac{\Delta R_c}{R_c} = \frac{R_c - R_{roll}}{R_c} \ll 1, \quad (32)$$

as mentioned above. On the other hand, matching ϕ in Eqs. (27) and (29) at $r = R_c$ gives

$$C_\infty \simeq (\phi_c - \phi_\infty) R_c. \quad (33)$$

The two C_∞ in Eqs. (31) and (33) must be equal. Introducing the Newtonian potential at the surface of the object $\Phi_c \equiv -GM_c/R_c < 0$, we have

$$\frac{\Delta R_c}{R_c} = \frac{\phi_c - \phi_\infty}{6\beta M_{pl} |\Phi_c|} \cdot m_\infty R_c \ll 1, \quad (34)$$

which means that

$$\frac{\phi_c - \phi_\infty}{6\beta M_{pl} |\Phi_c|} \ll \frac{1}{m_\infty R_c} \ll 1, \quad (35)$$

since $m_\infty R_c \gg 1$ as mentioned above. Substituting Eq. (31) into Eq. (29), we find the exterior solution

$$\phi(r) \simeq \frac{\beta}{4\pi M_{pl}} \frac{1}{m_\infty R_c} \left(\frac{3\Delta R_c}{R_c} \right) \frac{M_c e^{-m_\infty(r-R_c)}}{r} + \phi_\infty \quad \text{for } r > R_c. \quad (36)$$

Clearly, there are double suppressions $\Delta R_c/R_c \ll 1$ and $1/(m_\infty R_c) \ll 1$ before the Yukawa-suppression in Eq. (36). Thus, $\phi \simeq \phi_\infty$ soon after $r \gtrsim R_c$, and hence the fifth-force mediated by the scalar field ϕ is nearly zero. We can see the thin-shell effect on the other hand. As mentioned above, Eq. (5) still holds in the inverse chameleon mechanism. The strength of fifth-force is characterized by

$$\mathbf{a}_\phi = -\nabla \ln A(\phi) = -\frac{\beta}{M_{pl}} \nabla \phi, \quad (37)$$

while the strength of gravitational force is characterized by $\mathbf{a}_g = -\nabla \Phi_N$. Noting that Φ_c is the Newtonian potential at the surface of the object, Eq. (35) indicates that the fifth-force is extremely smaller than the gravitational force. The physical reason for the thin-shell effect has been mentioned at the end of Sec. II. That is, the fifth-force range $m_c^{-1} \ll R_c$, and hence the contribution from the core to the exterior profile is significantly suppressed. Only the contribution from a thin shell beneath the surface contributes considerably to the exterior profile. On the other hand, gravity couples to the entire bulk of the object. Thus, the fifth-force mediated by the scalar field ϕ on an exterior test particle is suppressed compared to the gravitational force. The thin-shell effect is the key to evade the fifth-force tests.

C. The thick shell regime

Let us turn to the thick shell regime. In this case, $\phi_i \lesssim \phi_c$, namely the scalar field at $r = 0$ is sufficiently displaced from ϕ_c . There is no “friction-dominated” region, since the “driving term” $-V_{\text{eff},\phi}$ is large at ϕ_i , as shown in the right panel of Fig. 1. So, the “particle” begins to roll almost as soon as it is released at $r = 0$. Similar to the case of chameleon mechanism [42, 43], the interior solution can be obtained by taking the $R_{roll} \rightarrow 0$ limit of Eq. (27) and replacing ϕ_c by ϕ_i , namely

$$\phi(r) \simeq -\frac{\beta \rho_c r^2}{6M_{pl}} + \phi_i \quad \text{for } 0 < r < R_c. \quad (38)$$

At $r = R_c$, the matter density ρ jumps from ρ_c to ρ_∞ , and ϕ changes to climb up the new V_{eff} with $\rho = \rho_\infty$, as shown in the left panel of Fig. 1. As mentioned above, there is a considerable transition region in the case of thick shell regime, because $\phi(r = R_c)$ can be sufficiently far from ϕ_∞ , unlike the thin shell regime. As mentioned in the last paragraph of Sec. IV A, in the transition region $R_c < r < R_t$, $-V_{\text{eff},\phi} \not\approx 0$, but it is much less than the “friction” $(2/r) d\phi/dr$ due to the relatively large “speed” $d\phi/dr$. In this case, Eq. (21) can be approximated by

$$\nabla^2 \phi = \frac{d^2 \phi}{dr^2} + \frac{2}{r} \frac{d\phi}{dr} \simeq 0, \quad (39)$$

while $-V_{\text{eff},\phi} \not\approx 0$ (including its first order term $\propto -V_{\text{eff},\phi}$) is completely neglected. Its solution reads

$$\phi(r) \simeq \frac{C_t}{r} + \phi_t, \quad (40)$$

where C_t and ϕ_t are both integration constants, which can be determined by requiring $d\phi/dr$ and ϕ are continuous at $r = R_c$. Matching $d\phi/dr$ from Eqs. (38) and (40) at $r = R_c$ gives

$$C_t = \frac{\beta \rho_c R_c^3}{3M_{pl}} = \frac{\beta M_c}{4\pi M_{pl}}. \quad (41)$$

So, the solution in the transition region is given by

$$\phi(r) \simeq \frac{\beta}{4\pi M_{pl}} \frac{M_c}{r} + \phi_t \quad \text{for } R_c < r < R_t. \quad (42)$$

Matching ϕ in Eqs. (38) and (42) at $r = R_c$ leads to

$$\phi_i - \phi_t = 3\beta M_{pl} |\Phi_c|, \quad (43)$$

and hence the integration constant ϕ_t is known. As mentioned in the last paragraph of Sec. IV A, at $r > R_t$, ϕ becomes fairly close to ϕ_∞ , while $-V_{\text{eff},\phi} \simeq 0$ indeed. At this stage, the “acceleration” $d^2\phi/dr^2$ and the “speed” $d\phi/dr$ tend to 0 (accordingly the “friction” $(2/r)d\phi/dr$ also tends to 0), so that the first order approximation of $-V_{\text{eff},\phi} \simeq 0$, i.e. $-V_{\text{eff},\phi\phi}(\phi - \phi_\infty) = m_\infty^2(\phi - \phi_\infty)$, makes sense. Noting that ϕ is very close to ϕ_∞ , Eq. (21) becomes

$$\nabla^2\phi = \frac{d^2\phi}{dr^2} + \frac{2}{r}\frac{d\phi}{dr} = -V_{\text{eff},\phi} = -V_{\text{eff},\phi}(\phi_\infty) - V_{\text{eff},\phi\phi}(\phi_\infty)(\phi - \phi_\infty) + \dots \simeq m_\infty^2(\phi - \phi_\infty), \quad (44)$$

whose solution (satisfying the boundary condition in Eq. (23)) is given by

$$\phi(r) \simeq \frac{C_\infty e^{-m_\infty(r-R_c)}}{r} + \phi_\infty. \quad (45)$$

The two unknowns C_∞ and R_t can be determined by requiring $d\phi/dr$ and ϕ are continuous at $r = R_t$. Matching ϕ in Eqs. (42) and (45) at $r = R_t$ gives

$$\frac{\beta}{4\pi M_{pl}} \frac{M_c}{R_t} + \phi_t \simeq \phi_\infty, \quad (46)$$

where we have neglected the first term in the right hand side of Eq. (45), because $\phi(r = R_t)$ is very close to ϕ_∞ by definition of R_t . From Eq. (46), it is easy to see that $\phi_t < \phi_\infty$ is on the left side of ϕ_∞ . This has no problem since ϕ_t is just an integration constant without special meaning in physics, as mentioned above. Substituting Eq. (43) into Eq. (46), we have

$$R_t = \frac{2}{3} R_c \left(1 - \frac{\phi_i - \phi_\infty}{3\beta M_{pl} |\Phi_c|} \right)^{-1}. \quad (47)$$

Noting $R_t > R_c > 0$, it is easy to see that

$$\frac{1}{3} < \frac{\phi_i - \phi_\infty}{3\beta M_{pl} |\Phi_c|} < 1. \quad (48)$$

Clearly, the width of transition region $\Delta_t = R_t - R_c$ can be fairly large for suitable ϕ_i . On the other hand, from Eq. (48) we find

$$\frac{\phi_c - \phi_\infty}{6\beta M_{pl} |\Phi_c|} > \frac{\phi_i - \phi_\infty}{6\beta M_{pl} |\Phi_c|} > \frac{1}{6}, \quad (49)$$

which implies that the thin shell condition in Eqs. (34) or (35) does not hold in the thick shell regime, as expected. Matching $d\phi/dr$ from Eqs. (42) and (45) at $r = R_t$ gives

$$C_\infty = \frac{\beta}{4\pi M_{pl}} \frac{M_c}{1 + m_\infty R_t} e^{-m_\infty(R_c - R_t)}. \quad (50)$$

Substituting Eq. (50) into Eq. (45), we have the exterior solution

$$\phi(r) \simeq \frac{\beta}{4\pi M_{pl}} \frac{M_c}{1 + m_\infty R_t} \frac{e^{-m_\infty(r-R_t)}}{r} + \phi_\infty \quad \text{for } r > R_t. \quad (51)$$

Note that m_∞ is fairly large if the background density ρ_∞ is fairly low, and hence there is another suppression factor $1/(1 + m_\infty R_t) \simeq 1/(m_\infty R_t) \ll 1$ before the Yukawa-suppression in Eq. (51). Thus, $\phi \simeq \phi_\infty$ soon after $r \gtrsim R_t$, and hence the fifth-force mediated by the scalar field ϕ is nearly zero (n.b. Eq. (37)). This can be easily understood in physics. In the case of thick shell regime, the fifth-force range $m_c^{-1} \gg R_c$, and hence the entire bulk of the object contributes significantly to the exterior profile. Although the fifth-force range $m_c^{-1} \gg R_c$, it is still finite. So, the contribution from the object extends up to $r \sim R_t$ at the most, but it is significantly suppressed at $r \gtrsim R_t$. The interesting region is $r < R_t$. In the transition region $R_c < r < R_t$, the corresponding $\phi(r)$ solution is given by Eq. (42), while the

Newtonian potential $\Phi_N \simeq -GM_c/r$ from Eq. (6) with $A(\phi) \simeq 1$ for $\beta\phi/M_{pl} \ll 1$. Substituting them into Eq. (5), we obtain the acceleration felt by a test particle in the transition region $R_c < r < R_t$,

$$\mathbf{a} = -\nabla(\Phi_N + \ln A(\phi)) \simeq -\frac{GM_c}{r^2} \mathbf{e}_r - \frac{\beta}{M_{pl}} \frac{d\phi}{dr} \mathbf{e}_r \simeq -\frac{GM_c}{r^2} (1 - 2\beta^2) \mathbf{e}_r, \quad (52)$$

which means that the gravitational force is considerably weakened by the fifth-force mediated by the scalar field ϕ . It is equivalent to a weakened gravitational force with $G_{\text{eff}} = (1 - 2\beta^2)G$. So, it is possible to test the fifth-force in the transition region outside the object in thick shell regime, such as compact stars including white dwarfs and neutron stars. On the other hand, inside the object $r < R_c$, the interior $\phi(r)$ solution is given by Eq. (38), while the Newtonian potential $\Phi_N \simeq -(2\pi G\rho_c/3)(3R_c^2 - r^2)$ from Eq. (6) with $A(\phi) \simeq 1$ for $\beta\phi/M_{pl} \ll 1$. Substituting them into Eq. (5), we obtain the acceleration felt by a test particle inside the object $r < R_c$, namely

$$\mathbf{a} = -\nabla(\Phi_N + \ln A(\phi)) \simeq -\frac{4\pi G\rho_c}{3} \mathbf{r} - \frac{\beta}{M_{pl}} \frac{d\phi}{dr} \mathbf{e}_r \simeq -\frac{4\pi G\rho_c}{3} (1 - 2\beta^2) \mathbf{r}. \quad (53)$$

It is also equivalent to a weakened gravitational force with $G_{\text{eff}} = (1 - 2\beta^2)G$ inside the object in thick shell regime. So, it is possible to increase the mass limits for compact stars such as white dwarfs and neutron stars. Noting that β can be $\mathcal{O}(1)$, the effect of fifth-force could be fairly significant.

V. MASS LIMITS FOR COMPACT STARS IN THE INVERSE CHAMELEON MECHANISM

A. White dwarfs

Here, we consider the mass limits for compact stars in the inverse chameleon mechanism. As shown above, the gravitational force is considerably weakened by the fifth-force mediated by the scalar field ϕ inside a compact object in thick shell regime. However, the object is assumed to be homogeneous in Sec. IV, since its main goal is to show how to evade the fifth-force tests on earth and in solar system where a homogeneous object is a good enough approximation. As is well known, compact stars such as white dwarfs and neutron stars are highly inhomogeneous. So, we cannot directly use the results of Sec. IV, for example, $G_{\text{eff}} = (1 - 2\beta^2)G$. Instead, here we should consider compact stars in general, without assuming homogeneity.

At first, we consider white dwarfs. As is well known, one can use the Newtonian approximation for the calculation of white dwarf structure [1–3]. For a spherical star, the mass interior to a radius r is given by

$$M(r) = \int_0^r 4\pi\tilde{r}^2 \rho(\tilde{r}) d\tilde{r}, \quad \text{or} \quad \frac{dM(r)}{dr} = 4\pi r^2 \rho(r). \quad (54)$$

We assume that the star is in a hydrostatic equilibrium. We consider an infinitesimal fluid element lying between r and $r + dr$, which has an area dS perpendicular to the radial direction, and a mass dm . The net outward pressure force on dm is

$$P(r) dS - P(r + dr) dS = -dP dS = -\frac{dP}{dr} dr dS. \quad (55)$$

On the other hand, using Eq. (5), the gravitational force and the fifth-force mediated by the scalar field ϕ on dm is given by

$$\mathbf{a} dm = -\nabla(\Phi_N + \ln A) dm, \quad (56)$$

while $-\nabla\Phi_N \simeq -(GM(r)/r^2) \mathbf{e}_r$ from Eq. (6) with $A(\phi) \simeq 1$ for $\beta\phi/M_{pl} \ll 1$, and $M(r)$ is given by Eq. (54), $A(\phi)$ is given by Eq. (13). Thus, in equilibrium we have

$$-\frac{dP}{dr} dr dS = \left(\frac{GM(r)}{r^2} + \frac{\beta}{M_{pl}} \frac{d\phi}{dr} \right) dm, \quad (57)$$

which is equivalent to

$$\frac{dP}{dr} = -\rho \left(\frac{GM(r)}{r^2} + \frac{\beta}{M_{pl}} \frac{d\phi}{dr} \right). \quad (58)$$

Using Eq. (54), we can recast Eq. (58) as

$$\frac{1}{r^2} \frac{d}{dr} \left(\frac{r^2}{\rho} \frac{dP}{dr} \right) = -4\pi G\rho - \frac{\beta}{M_{pl}} \nabla^2 \phi. \quad (59)$$

Substituting Eq. (11) or Eq. (21) into Eq. (59), and noting $|V_{,\phi}| \ll A_{,\phi} \rho$ inside the object in thick shell regime (as mentioned in Sec. IV), we obtain (see also the note in [50] for an alternative derivation)

$$\frac{1}{r^2} \frac{d}{dr} \left(\frac{r^2}{\rho} \frac{dP}{dr} \right) = -4\pi G\rho (1 - 2\beta^2) = -4\pi G_{\text{eff}} \rho, \quad (60)$$

where we have used $\beta\phi/M_{pl} \ll 1$. Now, we arrive at the same position of the usual calculation of white dwarf structure [1–3] but with an effective gravitational constant

$$G_{\text{eff}} = (1 - 2\beta^2) G. \quad (61)$$

Notice that the above derivations hold for the general $\rho = \rho(r)$, without assuming homogeneity. Following e.g. [1–3, 7], we can easily derive the mass limit for white dwarfs. We consider a polytropic equation of state (EOS) for the fermion gas (the electron gas),

$$P = K\rho^\Gamma = K\rho^{1+1/n}, \quad (62)$$

where K , n , $\Gamma = 1 + 1/n$ are constants, and n is the so-called polytropic index. It is convenient to introduce the dimensionless variables θ and ξ by the parameterizations

$$\rho = \rho_0 \theta^n, \quad r = \alpha \xi, \quad (63)$$

where $\rho_0 \equiv \rho(r=0)$ is the central density, and

$$\alpha^2 \equiv \frac{(n+1) K \rho_0^{1/n-1}}{4\pi G_{\text{eff}}}. \quad (64)$$

Using these dimensionless variables, the hydrostatic equilibrium equation (60) can be recast as the well-known Lane-Emden equation [1–3, 7]

$$\frac{1}{\xi^2} \frac{d}{d\xi} \left(\xi^2 \frac{d\theta}{d\xi} \right) = -\theta^n. \quad (65)$$

It can be numerically solved with the boundary conditions at the center, namely

$$\theta = 1, \quad \theta' = 0 \quad \text{at} \quad \xi = 0, \quad (66)$$

where $\theta' = d\theta/d\xi$. The surface of the star (where $P = \rho = 0$) is located at $\theta(\xi_*) = 0$. Eq. (65) can be integrated numerically, starting at $\xi = 0$ with the boundary conditions in Eq. (66). For $n < 5$, the solutions decrease monotonically and have a zero at a finite value ξ_* . For various polytropic EOS, the corresponding ξ_* and $\xi_*^2 |\theta'(\xi_*)|$ can be found in this way. For example, in the non-relativistic case ($\Gamma = 5/3$ or $n = 3/2$), one find [1–3, 7]

$$\xi_* = 3.6537, \quad \xi_*^2 |\theta'(\xi_*)| = 2.71406. \quad (67)$$

In the extreme relativistic case ($\Gamma = 4/3$ or $n = 3$), they are [1–3, 7]

$$\xi_* = 6.89685, \quad \xi_*^2 |\theta'(\xi_*)| = 2.01824. \quad (68)$$

With ξ_* , we obtain the stellar radius R_* as a function of the central density

$$R_* = \alpha \xi_* = \sqrt{\frac{(n+1)K}{4\pi G_{\text{eff}}}} \rho_0^{(1-n)/(2n)} \xi_*, \quad (69)$$

and the stellar mass M_* as a function of the central density

$$\begin{aligned} M_* &= \int_0^{R_*} 4\pi r^2 \rho dr = 4\pi \alpha^3 \rho_0 \int_0^{\xi_*} \xi^2 \theta^n d\xi = -4\pi \alpha^3 \rho_0 \int_0^{\xi_*} \frac{d}{d\xi} \left(\xi^2 \frac{d\theta}{d\xi} \right) d\xi \\ &= 4\pi \alpha^3 \rho_0 \xi_*^2 |\theta'(\xi_*)| = 4\pi \left[\frac{(n+1)K}{4\pi G_{\text{eff}}} \right]^{3/2} \rho_0^{(3-n)/(2n)} \xi_*^2 |\theta'(\xi_*)|. \end{aligned} \quad (70)$$

Eliminating the central density ρ_0 in Eqs. (69) and (70), we obtain the mass-radius relation as

$$M_*(R_*) = 4\pi R_*^{(3-n)/(1-n)} \left[\frac{(n+1)K}{4\pi G_{\text{eff}}} \right]^{n/(n-1)} \xi_*^2 |\theta'(\xi_*)| \xi_*^{(3-n)/(1-n)}. \quad (71)$$

For various polytropic EOS, the corresponding K have been given in e.g. [1–3, 7]. We are interested in the extreme relativistic case ($\Gamma = 4/3$ or $n = 3$) which gives the mass limit for white dwarfs. Noting Eq. (71), the stellar mass M_* is independent of radius R_* in this case, namely

$$M_* = (1 - 2\beta^2)^{-3/2} M_{\text{Ch}} = (1 - 2\beta^2)^{-3/2} 1.457 M_{\odot} \left(\frac{2}{\mu_e} \right)^2, \quad (72)$$

where we have used Eq. (61), and μ_e is the mean molecular weight per electron (usually $\mu_e \simeq 2$ for white dwarfs, but it is larger for different chemical compositions). From Eq. (72), it is easy to see that the mass limit for white dwarfs becomes $(1 - 2\beta^2)^{-3/2}$ times the well-known Chandrasekhar limit M_{Ch} . On the other hand, from Eq. (69), the corresponding stellar radius R_* is given by

$$R_* = (1 - 2\beta^2)^{-1/2} R_{\text{Ch}} = (1 - 2\beta^2)^{-1/2} 3.347 \times 10^4 \text{ km} \left(\frac{\rho_0}{10^6 \text{ g/cm}^3} \right)^{-1/3} \left(\frac{2}{\mu_e} \right)^{2/3}, \quad (73)$$

which is also increased by a factor $(1 - 2\beta^2)^{-1/2}$. Of course, we should require $\beta^2 < 1/2$. Noting that β can be $\mathcal{O}(1)$ in the inverse chameleon mechanism, the mass limit for white dwarfs could be significantly increased. For example, the mass limit for white dwarfs becomes about 1.66, 1.84, 2.15, 2.83, 3.95, 5.2, 6.75, 11.2 times the Chandrasekhar limit mass M_{Ch} for $\beta^2 = 1/7, 1/6, 1/5, 1/4, 0.3, 1/3, 0.36, 2/5$, respectively. In fact, it can be larger than $3M_{\odot}$ for $\beta^2 \gtrsim 1/5$, and hence the super-Chandrasekhar mass white dwarfs can be easily accommodated. In principle, the mass limit for white dwarfs can be very high for β^2 close enough to $1/2$. However, the value of β^2 will be constrained by observations (see discussions in Sec. VI), and hence the mass limit for white dwarfs cannot be arbitrarily large in practice.

B. Other compact stars

In the case of white dwarfs, the Newtonian approximation is good enough. However, in the cases of neutron stars and other relativistic stars, the full relativistic hydrostatic equilibrium should be considered instead (see e.g. [1–3]). The Tolman-Oppenheimer-Volkoff (TOV) equation is the corresponding master equation. On the other hand, the realistic (non-analytic) EOS should be considered, but which is not so clear to date. In the cases of neutron stars (and other relativistic stars), numerical computer codes are commonly employed. Therefore, it is not straightforward to obtain a simple factor increasing the mass limits (like the factor $(1 - 2\beta^2)^{-3/2}$ in the case of white dwarfs).

However, we argue that the mass limits for neutron stars and other relativistic stars will also be considerably increased in the inverse chameleon mechanism. At first, we have clearly shown that the fifth-force mediated by the scalar field ϕ will notably weaken the gravitational force inside the object

in thick shell regime. The compact stars are stable due to the balance between gravitational force and degeneracy pressure. When the gravitational force is significantly weakened by the fifth-force, the same degeneracy pressure can of course support a much heavier mass. On the other hand, we note that compact stars are in a sequence, as is well known. If electron degeneracy pressure can support a white dwarf with a mass $M > 3M_\odot$, $5M_\odot$ or even higher (for larger β^2), it certainly will not collapse into a neutron star or other relativistic stars such as quark star and gravastar. So, the mass limits for neutron stars and other relativistic stars must exceed the one for white dwarfs. While the mass limit for white dwarfs is significantly increased by a factor $(1 - 2\beta^2)^{-3/2}$, the mass limits for neutron stars and other relativistic stars can only be increased accordingly or even dramatically.

VI. CONCLUDING REMARKS

As is well known, there are various mass limits for compact stars. For example, the maximum mass for non-rotating white dwarfs is given by the famous Chandrasekhar limit about $1.4M_\odot$. Although the mass limit for neutron stars is not so clear to date, one of the widely accepted values is about $2.1M_\odot$. Recently, challenges to these mass limits appeared. Motivated by the super-Chandrasekhar mass white dwarfs with masses up to $2.4 \sim 2.8M_\odot$, and compact objects (probably neutron stars) in the mass gap (from $2.5M_\odot$ or $3M_\odot$ to $5M_\odot$) inferred from gravitational waves detected by LIGO/Virgo in the third observing run (O3), we reconsider the mass limits for compact stars in the present work. Without invoking strong magnetic field and/or exotic EOS, we try to increase the mass limits for compact stars in modified gravity theory. In this work, we propose an inverse chameleon mechanism, and show that the fifth-force mediated by the scalar field can evade the severe tests on earth, in solar system and universe, but manifest itself in compact stars such as white dwarfs and neutron stars. The mass limits for compact stars in the inverse chameleon mechanism can be easily increased to $3M_\odot$, $5M_\odot$ or even larger.

In the literature, strong magnetic field and/or exotic EOS are frequently invoked in many scenarios to increase the mass limits for compact stars. On the other hand, the mass limits can also be increased for rigidly spinning compact stars (see e.g. [55]). However, the $2.6M_\odot$ compact object found by LIGO/Virgo in GW190814 event has low primary spin [28]. As shown in this work, we consider that the scenarios employing modified gravity theories deserve further investigation.

In this work, a non-canonical scalar field (akin to phantom) is used in our inverse chameleon mechanism, and hence the gravitational force is weakened by the fifth-force mediated by the scalar field, n.b. the effective gravitational constant $G_{\text{eff}} = (1 - 2\beta^2)G$. In fact, one can instead consider a different inverse chameleon mechanism still using a canonical scalar field (akin to quintessence), and the action takes the same form given in Eq. (1), but $V(\phi) = \mathcal{M}^{4-s} \phi^s$ with $1 < s < 2$, and $A(\phi) = \exp(-\beta\phi/M_{pl})$ with $\beta > 0$. In this case, $m_\phi^2 = V_{\text{eff},\phi\phi}(\phi_{\text{min}}) \propto \rho^{(s-2)/(s-1)}$ is also a decreasing function of the local matter density ρ . Unfortunately, the gravitational force is instead strengthened by the fifth-force mediated by the scalar field, with $G_{\text{eff}} = (1 + 2\beta^2)G$. So, it fails to increase the mass limits for compact stars. But we still mention it here with the hope to revive it for another completely different goal in the future.

Actually, one can see that $G_{\text{eff}} = (1 + 2\beta^2)G$ in both cases of the original chameleon mechanism and the inverse chameleon mechanism with a canonical scalar field (akin to quintessence) mentioned above. In both cases, the fifth-force mediated by a canonical scalar field (akin to quintessence) is attractive, as is well known in quantum field theory (QFT). However, it is not the case of our inverse chameleon mechanism with a non-canonical scalar field (akin to phantom) proposed in the present work. In fact, it was shown in [56] that the phantom scalar field mediates a long-range repulsive force surprisingly. This is mainly due to the negative kinetic term of the phantom scalar field. So, it is easy to understand $G_{\text{eff}} = (1 - 2\beta^2)G$ in our inverse chameleon mechanism, while $-2\beta^2$ indicates the long-range repulsive fifth-force mediated by the non-canonical scalar field (akin to phantom).

The phantom scalar field with a negative kinetic term has led many interesting features (significantly different from the ones of canonical scalar field) to cosmology in the past two decades. On the other hand, it is worth noting that phantom dark energy whose EOS parameter $w < -1$ is slightly favored by the cosmological observations (e.g. $w = -1.03 \pm 0.03$ from the Planck 2018 results [57]). Therefore, it is well motivated to also consider a non-canonical scalar field (akin to phantom) in astrophysics. Note that it was argued in e.g. [58–60] that phantom could avoid the quantum instability in the ultraviolet region. One can try to make the instability time scale greater than the age of the universe. However,

phantom within a Lorentz invariant framework might be experimentally excluded [58]. As is argued in e.g. [58], in order to keep the instability at unobservable levels, a Lorentz-violating ultraviolet cutoff Λ must be applied to low-energy effective theories of phantom. It was found in [58] that the cutoff Λ is constrained by observations of the diffuse gamma-ray background, namely $\Lambda \lesssim 3 \text{ MeV}$. As an explicit and simple example, we can consider a Lorentz-violating Lagrangian $\frac{1}{2}(\partial\phi)^2 - \frac{1}{2}\Lambda^{-2}(\nabla^2\phi)^2$ mentioned in [58] (see also e.g. [62]). The second term is the key to keep the instability at unobservable levels, and it makes sense in the high-energy region above the cutoff Λ . On the other hand, in the low-energy region well below the cutoff Λ , the Lagrangian $\frac{1}{2}(\partial\phi)^2 - \frac{1}{2}\Lambda^{-2}(\nabla^2\phi)^2$ effectively reduces to $\frac{1}{2}(\partial\phi)^2$, namely the one used in Eq. (10) of the present work. As is shown in Sec. III B, the mass of phantom field ϕ is about $\mathcal{O}(10^{-3} \text{ eV})$ in the inverse chameleon mechanism, which is much lower than the cutoff $\Lambda \lesssim 3 \text{ MeV}$. Thus, as a low-energy effective theory, one needs not worry about the quantum instability in the inverse chameleon mechanism. Note that Lorentz violation has been induced in many theories. For example, most theories of quantum gravity (QG) commonly predict that Lorentz violation might happen on high-energy scales. In fact, the observational hints for Lorentz violation were found in e.g. [61] by using the time-lag data of gamma-ray bursts (GRBs). Of course, the debate about quantum instability of phantom is still not completely settled in the literature by now, and we consider that it is better to keep an open mind to such kind of theories using a non-canonical scalar field (akin to phantom).

Note that β is a constant in this work. So, the passage from $1 - 2\beta^2 > 0$ to $1 - 2\beta^2 < 0$ and vice versa cannot happen. Of course, it is interesting to consider a varying β in some modified versions of the inverse chameleon mechanism, but this is beyond the scope of the present work. In principle, $1 - 2\beta^2 < 0$ can be allowed, and $G_{\text{eff}} = (1 - 2\beta^2)G < 0$ means that the repulsive fifth-force mediated by a non-canonical scalar field (akin to phantom) overcomes gravity. However, it is worth noting that $G_{\text{eff}} = (1 - 2\beta^2)G$ holds only in the cases of compact stars where the matter density is very high. As shown in this work, the inverse chameleon mechanism hides itself on earth, in solar system and universe, where the matter density is low. Thus, the usual stars (e.g. sun, stellar objects, planets, moons) and most objects in the universe can still be formed and exist as in GR. Nothing changes in the cases of low matter density even if $1 - 2\beta^2 < 0$. Only in the cases of very high matter density, the inverse chameleon mechanism manifests itself, and then $1 - 2\beta^2 < 0$ will prevent the existence of compact stars such as white dwarfs and neutron stars. On the contrary, the observational fact that white dwarfs and neutron stars do exist must require $1 - 2\beta^2 > 0$. In other words, $\beta^2 < 1/2$ must be constrained by the observations.

A natural question is how to test the inverse chameleon mechanism. On the other hand, in principle, the mass limits can be arbitrarily large by using $\beta^2 \rightarrow 1/2$ in the factor $(1 - 2\beta^2)^{-3/2}$. Of course, this cannot happen in a reasonable theory. A constraint on β^2 must be set from observations and/or experiments. Since the inverse chameleon mechanism hides itself on earth, in solar system and universe, it cannot be tested here. The inverse chameleon mechanism manifests itself in or near compact stars such as white dwarfs and neutron stars. The discovery of exoplanets shared the 2019 Nobel Prize in Physics. In fact, the first two exoplanets announced in 1992 are orbiting a pulsar (neutron star) [51]. To date, some exoplanets orbiting white dwarfs and neutron stars have been found [52–54, 63]. As shown in Sec. IV C, there is a transition region $R_c < r < R_t$ outside compact stars, where $G_{\text{eff}} = (1 - 2\beta^2)G$. The exoplanets inside the transition region $R_c < r < R_t$ feels a weakened gravitational force, and hence their orbits will be affected. So, the observations of exoplanets orbiting compact stars such as white dwarfs and neutron stars might be used to test the inverse chameleon mechanism, and set a constraint on β^2 . However, since the semi-major axes of the detected exoplanets orbiting white dwarfs and neutron stars are usually too large while the transition regions outside compact stars are not so wide, no considerable constraints can be made to date. We hope that an exoplanet very close to compact star can be found in the future. Another type of tests might come from gravitational waves. Two compact stars are very close in the last stage of their coalescence, so that they enter the transition regions of each other, where the gravitational force is notably weakened by the fifth-force mediated by the scalar field. In the last stage of the coalescence of binary neutron star, neutron star – black hole, neutron star – white dwarf, white dwarf – black hole, and binary white dwarf, the inverse chameleon mechanism will affect these two compact stars at a very short distance. Thus, gravitational waves from the last stage of binary compact star coalescence might carry the information about the inverse chameleon mechanism. We encourage the GW community to search it in the GW data.

ACKNOWLEDGEMENTS

We thank the anonymous referee for useful comments and suggestions, which helped us to improve this work. We are grateful to Zong-Kuan Guo, Shupeng Song, Shou-Long Li, Jing-Yi Jia, Da-Chun Qiang, Hua-Kai Deng and Han-Yue Guo for kind help and discussions. This work was supported in part by NSFC under Grants No. 11975046 and No. 11575022.

-
- [1] M. Camenzind, *Compact Objects in Astrophysics: White Dwarfs, Neutron Stars and Black Holes*, Springer-Verlag, Berlin (2007).
 - [2] S. L. Shapiro and S. A. Teukolsky, *Black Holes, White Dwarfs, and Neutron Stars: The Physics of Compact Objects*, Wiley-VCH, Weinheim (2004).
 - [3] N. K. Glendenning, *Compact Stars: Nuclear Physics, Particle Physics and General Relativity*, Springer, New York (1996).
 - [4] S. Chandrasekhar, *Astrophys. J.* **74**, 81 (1931).
 - [5] S. Chandrasekhar and E. A. Milne, *Mon. Not. Roy. Astron. Soc.* **91**, no. 5, 456 (1931).
 - [6] S. Chandrasekhar, *Mon. Not. Roy. Astron. Soc.* **95**, 207 (1935).
 - [7] S. Chandrasekhar, *An Introduction to the Study of Stellar Structure*, The University of Chicago Press (1939); republished by Dover Publications (1967) and (2010).
 - [8] F. Özel and P. Freire, *Ann. Rev. Astron. Astrophys.* **54**, 401 (2016) [arXiv:1603.02698].
 - [9] F. Özel *et al.*, *Astrophys. J.* **757**, 55 (2012) [arXiv:1201.1006].
 - [10] N. Chamel *et al.*, *Int. J. Mod. Phys. E* **22**, 1330018 (2013) [arXiv:1307.3995].
 - [11] L. Rezzolla, E. R. Most and L. R. Weih, *Astrophys. J. Lett.* **852**, L25 (2018) [arXiv:1711.00314].
 - [12] H. T. Cromartie *et al.*, *Nat. Astron.* **4**, no. 1, 72 (2019) [arXiv:1904.06759].
 - [13] A. Burrows (2017), <https://www.astro.princeton.edu/~burrows/classes/403/neutron.stars.pdf>
 - [14] V. Kalogera and G. Baym, *Astrophys. J. Lett.* **470**, L61 (1996) [astro-ph/9608059].
 - [15] D. A. Howell *et al.*, *Nature* **443**, 308 (2006) [astro-ph/0609616].
 - [16] U. Das and B. Mukhopadhyay, *Phys. Rev. Lett.* **110**, no. 7, 071102 (2013) [arXiv:1301.5965].
 - [17] I. Hachisu, M. Kato, H. Saio and K. Nomoto, *Astrophys. J.* **744**, 69 (2012) [arXiv:1106.3510].
 - [18] M. Santander-García *et al.*, *Nature* 519, no. 7541, 63 (2015) [arXiv:1609.00178].
 - [19] E. Y. Hsiao *et al.*, *Astrophys. J.* **900**, no. 2, 140 (2020) [arXiv:2008.05614].
 - [20] P. J. Brown *et al.*, *Astrophys. J.* **787**, 29 (2014) [arXiv:1404.0650].
 - [21] B. P. Abbott *et al.*, *Phys. Rev. Lett.* **116**, no. 6, 061102 (2016) [arXiv:1602.03837].
 - [22] B. P. Abbott *et al.*, *Phys. Rev. Lett.* **116**, no. 22, 221101 (2016) [arXiv:1602.03841].
 - [23] LIGO/Virgo Collaboration (2019), <https://emfollow.docs.ligo.org/userguide/content.html> and <https://emfollow.docs.ligo.org/userguide/glossary.html>
 - [24] <https://gcn.gsfc.nasa.gov/other/S191216ap.gcn3>
<https://gcn.gsfc.nasa.gov/other/GW191216ap.gcn3>
 - [25] <https://gracedb.ligo.org/superevents/S191216ap/>
 - [26] <https://gcn.gsfc.nasa.gov/other/S190814bv.gcn3>
<https://gcn.gsfc.nasa.gov/other/GW190814bv.gcn3>
 - [27] <https://gracedb.ligo.org/superevents/S190814bv/>
 - [28] R. Abbott *et al.*, *Astrophys. J. Lett.* **896**, no. 2, L44 (2020) [arXiv:2006.12611].
 - [29] <https://www.ligo.org/news/index.php#GW190814>
<https://www.ligo.org/detections/GW190814/pr-english.pdf>
 - [30] H. Wei and M. Z. Feng, *Commun. Theor. Phys.* **72**, no. 6, 065401 (2020) [arXiv:1912.03466];
H. Wei *et al.*, *Astrophys. Space Sci.* **365**, 148 (2020) [arXiv:1911.04201].
 - [31] U. Das and B. Mukhopadhyay, *JCAP* **1406**, 050 (2014) [arXiv:1404.7627].
 - [32] U. Das and B. Mukhopadhyay, *Phys. Rev. D* **86**, 042001 (2012) [arXiv:1204.1262].
 - [33] S. K. Roy *et al.*, *Phys. Rev. D* **100**, no. 6, 063008 (2019) [arXiv:1907.13480].
 - [34] Q. X. Zou and X. H. Meng, arXiv:1505.00859 [astro-ph.HE].
 - [35] H. Shah and K. Sebastian, *J. Mod. Phys.* **11**, no. 09, 1466 (2020).
 - [36] I. Bombaci, *Astron. Astrophys.* **305**, 871 (1996).

- [37] J. L. Zdunik and P. Haensel, *Astron. Astrophys.* **551**, A61 (2013) [arXiv:1211.1231].
- [38] D. A. Godzieba, D. Radice and S. Bernuzzi, *Astrophys. J.* **908**, no. 2, 122 (2021) [arXiv:2007.10999].
- [39] A. M. Studzińska *et al.*, *Mon. Not. Roy. Astron. Soc.* **463**, no. 3, 2667 (2016).
- [40] N. Chamel *et al.*, *Astron. Astrophys.* **553**, A22 (2013) [arXiv:1205.0983].
- [41] G. J. Olmo, D. Rubiera-Garcia and A. Wojnar, *Phys. Rept.* **876**, 1 (2020) [arXiv:1912.05202].
- [42] J. Khoury and A. Weltman, *Phys. Rev. Lett.* **93**, 171104 (2004) [astro-ph/0309300].
- [43] J. Khoury and A. Weltman, *Phys. Rev. D* **69**, 044026 (2004) [astro-ph/0309411].
- [44] P. Brax *et al.*, *Phys. Rev. D* **70**, 123518 (2004) [astro-ph/0408415].
- [45] S. S. Gubser and J. Khoury, *Phys. Rev. D* **70**, 104001 (2004) [hep-ph/0405231].
- [46] J. Khoury, *Class. Quant. Grav.* **30**, 214004 (2013) [arXiv:1306.4326].
- [47] H. Wei and R. G. Cai, *Phys. Rev. D* **71**, 043504 (2005) [hep-th/0412045].
- [48] J. Wang, L. Hui and J. Khoury, *Phys. Rev. Lett.* **109**, 241301 (2012) [arXiv:1208.4612].
- [49] R. R. Caldwell, *Phys. Lett. B* **545**, 23 (2002) [astro-ph/9908168].
- [50] Alternatively, we can derive Eq. (60) by using the Poisson equation for the Newtonian potential Φ_N given in Eq. (6). As is well known, $\nabla^2 f = (1/r^2) d(r^2 df/dr)/dr$ in spherical coordinates for any $f(r)$. In equilibrium, the total force, namely Eq. (55) plus Eq. (56), is zero. Thus, we have $-(1/\rho) dP/dr = \nabla(\Phi_N + \ln A) = d\Phi_N/dr + (\beta/M_{pl}) d\phi/dr$ for $A = \exp(\beta\phi/M_{pl})$. Substituting $d\Phi_N/dr = -(1/\rho) dP/dr - (\beta/M_{pl}) d\phi/dr$ into Eq. (6), and then using $\nabla^2\phi$ from Eq. (11) or Eq. (21) with $|V_{,\phi}| \ll A_{,\phi}\rho$, we finally obtain Eq. (60) for $\beta\phi/M_{pl} \ll 1$. In this alternative way, no explicit solutions for Φ_N and ϕ are required, and of course we need not assume that the object is homogeneous.
- [51] <https://en.wikipedia.org/wiki/Exoplanet>
- [52] https://en.wikipedia.org/wiki/White_dwarf#Debris_disks_and_planets
- [53] https://en.wikipedia.org/wiki/Neutron_star#Planets
https://en.wikipedia.org/wiki/Pulsar_planet
- [54] <https://exoplanetarchive.ipac.caltech.edu>
- [55] A. Halder *et al.*, *Phys. Rev. C* **103**, 035806 (2021) [arXiv:2005.14567].
- [56] L. Amendola, *Phys. Rev. Lett.* **93**, 181102 (2004) [hep-th/0409224].
- [57] N. Aghanim *et al.*, *Astron. Astrophys.* **641**, A6 (2020) [arXiv:1807.06209].
- [58] J. M. Cline, S. Jeon and G. D. Moore, *Phys. Rev. D* **70**, 043543 (2004) [hep-ph/0311312].
- [59] M. Libanov *et al.*, *JCAP* **0708**, 010 (2007) [arXiv:0704.1848].
- [60] M. Kaplinghat and A. Rajaraman, *Phys. Rev. D* **75**, 103504 (2007) [astro-ph/0601517].
- [61] X. B. Zou, H. K. Deng, Z. Y. Yin and H. Wei, *Phys. Lett. B* **776**, 284 (2018) [arXiv:1707.06367].
- [62] N. Arkani-Hamed *et al.*, *JHEP* **0405**, 074 (2004) [hep-th/0312099].
- [63] D. Veras, arXiv:2106.06550 [astro-ph.EP].